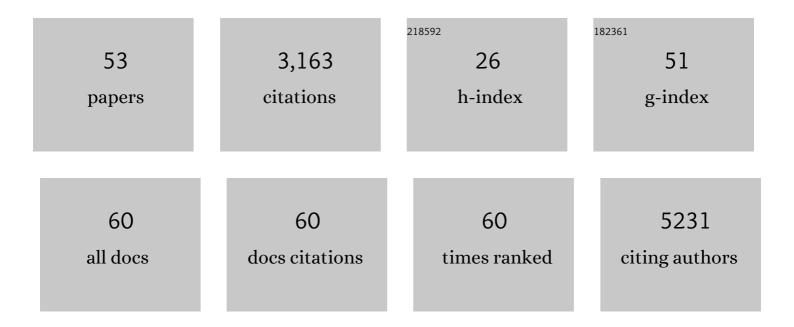
## Xiaoke Mu

List of Publications by Year in descending order

Source: https://exaly.com/author-pdf/7809924/publications.pdf Version: 2024-02-01



XIAOKE MIL

#	Article	IF	CITATIONS
1	Unveiling the Local Atomic Arrangements in the Shear Band Regions of Metallic Glass. Advanced Materials, 2021, 33, e2007267.	11.1	38
2	Unveiling local atomic bonding and packing of amorphous nanophases via independent component analysis facilitated pair distribution function. Acta Materialia, 2021, 212, 116932.	3.8	13
3	4D-STEM: Combining Pair Distribution Mapping and Multivariate Statistic Analysis to Quantify Structures in Complex Nanoscale Glasses. Microscopy and Microanalysis, 2021, 27, 1788-1790.	0.2	0
4	New Insight into Desodiation/Sodiation Mechanism of MoS <sub>2</sub> : Sodium Insertion in Amorphous Mo–S Clusters. ACS Applied Materials & Interfaces, 2021, 13, 40481-40488.	4.0	7
5	Quantifying the performance of a hybrid pixel detector with GaAs:Cr sensor for transmission electron microscopy. Ultramicroscopy, 2021, 227, 113298.	0.8	12
6	Grain boundary segregation induced precipitation in a non equiatomic nanocrystalline CoCuFeMnNi compositionally complex alloy. Acta Materialia, 2021, 220, 117281.	3.8	18
7	Understanding Structure Changes during Cycling of MoS2-based Mg Batteries. Microscopy and Microanalysis, 2019, 25, 2042-2043.	0.2	0
8	Towards quantitative treatment of electron pair distribution function. Acta Crystallographica Section B: Structural Science, Crystal Engineering and Materials, 2019, 75, 532-549.	0.5	38
9	4D-STEM Pair Distribution Function Mapping of the Morphology and Structure of Amorphous Organic Materials. Microscopy and Microanalysis, 2019, 25, 1944-1945.	0.2	1
10	Reversible control of magnetism: on the conversion of hydrated FeF <sub>3</sub> with Li to Fe and LiF. Journal of Materials Chemistry A, 2019, 7, 24005-24011.	5.2	6
11	Revealing the Dual Surface Reactions on a HE-NCM Li-Ion Battery Cathode and Their Impact on the Surface Chemistry of the Counter Electrode. ACS Applied Materials & Interfaces, 2019, 11, 6054-6065.	4.0	23
12	Mapping structure and morphology of amorphous organic thin films by 4D-STEM pair distribution function analysis. Microscopy (Oxford, England), 2019, 68, 301-309.	0.7	45
13	Electron Beam Effects on Oxide Thin Films—Structure and Electrical Property Correlations. Microscopy and Microanalysis, 2019, 25, 592-600.	0.2	23
14	(De)Lithiation Mechanism of Hierarchically Layered LiNi <sub>1/3</sub> Co <sub>1/3</sub> Mn <sub>1/3</sub> O <sub>2</sub> Cathodes during High-Voltage Cycling. Journal of the Electrochemical Society, 2019, 166, A5025-A5032.	1.3	27
15	Tuning the Curie temperature of Fe90Sc10 nanoglasses by varying the volume fraction and the composition of the interfaces. Scripta Materialia, 2019, 159, 109-112.	2.6	13
16	Lithium/Oxygen Incorporation and Microstructural Evolution during Synthesis of Liâ€Rich Layered Li[Li <sub>0.2</sub> Ni <sub>0.2</sub> Mn <sub>0.6</sub> ]O <sub>2</sub> Oxides. Advanced Energy Materials, 2019, 9, 1803094.	10.2	78
17	Low temperature structural stability of Fe <sub>90</sub> Sc <sub>10</sub> nanoglasses. Materials Research Letters, 2018, 6, 178-183.	4.1	4
18	Tailoring Surface Frustrated Lewis Pairs of In <sub>2</sub> O <sub>3â^`</sub> <i><sub>x</sub></i> (OH) <sub>y</sub> for Gasâ€Phase Heterogeneous Photocatalytic Reduction of CO <sub>2</sub> by Isomorphous Substitution of In <sup>3+</sup> with Bi <sup>3+</sup> . Advanced Science, 2018, 5, 1700732.	5.6	91

Χιάοκε Μυ

#	Article	IF	CITATIONS
19	Spectroscopic investigations on the origin of the improved performance of composites of nanoparticles/graphene sheets as anodes for lithium ion batteries. Carbon, 2018, 127, 47-56.	5.4	11
20	Fast kinetics of multivalent intercalation chemistry enabled by solvated magnesium-ions into self-established metallic layered materials. Nature Communications, 2018, 9, 5115.	5.8	114
21	Structure and Properties of Nanoglasses. Advanced Engineering Materials, 2018, 20, 1800404.	1.6	42
22	Solar Fuels: Tailoring Surface Frustrated Lewis Pairs of In <sub>2</sub> O <sub>3â``</sub> <i><sub>x</sub></i> (OH) <sub>y</sub> for Gasâ€Phase Heterogeneous Photocatalytic Reduction of CO <sub>2</sub> by Isomorphous Substitution of In <sup>3+</sup> with Bi <sup>3+</sup> (Adv. Sci. 6/2018). Advanced Science, 2018, 5, 1870034.	5.6	3
23	Role of surface spins on magnetization of Cr2O3 coated Î <sup>3</sup> -Fe2O3 nanoparticles. Solid State Sciences, 2018, 83, 43-48.	1.5	10
24	Activation and degradation of electrospun LiFePO4 battery cathodes. Journal of Power Sources, 2018, 396, 386-394.	4.0	21
25	Interlayerâ€Expanded Vanadium Oxychloride as an Electrode Material for Magnesiumâ€Based Batteries. ChemElectroChem, 2017, 4, 738-745.	1.7	22
26	Solution Growth of Ultralong Gold Nanohelices. ACS Nano, 2017, 11, 5538-5546.	7.3	30
27	Understanding the graphitization and growth of free-standing nanocrystalline graphene using in situ transmission electron microscopy. Nanoscale, 2017, 9, 12835-12842.	2.8	27
28	Cu-Zr nanoglasses: Atomic structure, thermal stability and indentation properties. Acta Materialia, 2017, 136, 181-189.	3.8	78
29	Radial Distribution Function Imaging by Diffraction Scanning Electron Microscopy. Microscopy and Microanalysis, 2016, 22, 488-489.	0.2	1
30	Secondâ€Harmonic Generation from ZnO/Al <sub>2</sub> O <sub>3</sub> Nanolaminate Optical Metamaterials Grown by Atomic‣ayer Deposition. Advanced Optical Materials, 2016, 4, 1203-1208.	3.6	19
31	VOCI as a Cathode for Rechargeable Chloride Ion Batteries. Angewandte Chemie, 2016, 128, 4357-4362.	1.6	26
32	Comparison of energy filtered TEM spectra image and automated crystal orientation mapping in LiFePO 4 /FePO 4 phase mapping. Microscopy and Microanalysis, 2016, 22, 1296-1297.	0.2	1
33	Surface segregation of primary glassy nanoparticles of Fe90Sc10 nanoglass. Materials Letters, 2016, 181, 248-252.	1.3	23
34	Radial distribution function imaging by STEM diffraction: Phase mapping and analysis of heterogeneous nanostructured glasses. Ultramicroscopy, 2016, 168, 1-6.	0.8	52
35	VOCl as a Cathode for Rechargeable Chloride Ion Batteries. Angewandte Chemie - International Edition, 2016, 55, 4285-4290.	7.2	81
36	Highâ€Performance Lowâ€Temperature Li <sup>+</sup> Intercalation in Disordered Rockâ€Salt Li–Cr–V Oxyfluorides. ChemElectroChem, 2016, 3, 892-895.	1.7	32

Χιάοκε Μυ

#	Article	IF	CITATIONS
37	Mechanical Milling Assisted Synthesis and Electrochemical Performance of High Capacity LiFeBO <sub>3</sub> for Lithium Batteries. ACS Applied Materials & Interfaces, 2016, 8, 2166-2172.	4.0	18
38	A highly N-doped carbon phase "dressing―of macroscopic supports for catalytic applications. Chemical Communications, 2015, 51, 14393-14396.	2.2	43
39	Macroscopic nanodiamonds/β-SiC composite as metal-free catalysts for steam-free dehydrogenation of ethylbenzene to styrene. Applied Catalysis A: General, 2015, 499, 217-226.	2.2	53
40	Investigating hybridization schemes of coupled split-ring resonators by electron impacts. Optics Express, 2015, 23, 20721.	1.7	7
41	Nanodiamond decorated few-layer graphene composite as an efficient metal-free dehydrogenation catalyst for styrene production. Catalysis Today, 2015, 249, 167-175.	2.2	45
42	Fast Li Storage in MoS <sub>2</sub> â€Graphene arbon Nanotube Nanocomposites: Advantageous Functional Integration of 0D, 1D, and 2D Nanostructures. Advanced Energy Materials, 2015, 5, 1401170.	10.2	155
43	Singleâ€Layered Ultrasmall Nanoplates of MoS <sub>2</sub> Embedded in Carbon Nanofibers with Excellent Electrochemical Performance for Lithium and Sodium Storage. Angewandte Chemie - International Edition, 2014, 53, 2152-2156.	7.2	826
44	Lithium Potential Variations for Metastable Materials: Case Study of Nanocrystalline and Amorphous LiFePO <sub>4</sub> . Nano Letters, 2014, 14, 5342-5349.	4.5	33
45	Influence of a Second Cation ( <i>M</i> = Ca <sup>2+</sup> , Mg <sup>2+</sup> ) on the Phase Evolution of (Ba <i><sub>x</sub>M</i> <sub>1â€"<i>x</i></sub> )F <sub>2</sub> Starting from Amorphous Deposits. Zeitschrift Fur Anorganische Und Allgemeine Chemie, 2014, 640, 1868-1875.	0.6	10
46	An FeF <sub>3</sub> ·0.5H <sub>2</sub> O Polytype: A Microporous Framework Compound with Intersecting Tunnels for Li and Na Batteries. Journal of the American Chemical Society, 2013, 135, 11425-11428.	6.6	177
47	Multichannel hollow TiO2 nanofibers fabricated by single-nozzle electrospinning and their application for fast lithium storage. Electrochemistry Communications, 2013, 28, 54-57.	2.3	43
48	Top-Down Synthesis of Open Framework Fluoride for Lithium and Sodium Batteries. Chemistry of Materials, 2013, 25, 962-969.	3.2	117
49	A Highâ€Capacity Cathode for Lithium Batteries Consisting of Porous Microspheres of Highly Amorphized Iron Fluoride Densified from Its Open Parent Phase. Advanced Energy Materials, 2013, 3, 113-119.	10.2	111
50	"Nanoâ€Pearlâ€6tring―TiNb <sub>2</sub> O <sub>7</sub> as Anodes for Rechargeable Lithium Batteries. Advanced Energy Materials, 2013, 3, 49-53.	10.2	220
51	Evolution of order in amorphous-to-crystalline phase transformation of MgF <sub>2</sub> . Journal of Applied Crystallography, 2013, 46, 1105-1116.	1.9	39
52	Hollow Carbon Nanospheres with a High Rate Capability for Lithiumâ€Based Batteries. ChemSusChem, 2012, 5, 400-403.	3.6	215
53	Structural Evolution of Magnesium Difluoride: from an Amorphous Deposit to a New Polymorph. Inorganic Chemistry, 2011, 50, 1563-1569.	1.9	20